Report:
for Nick Lancaster, DEES, Desert Research Institute, on behalf of the Great Basin Unified Air Pollution Control District.

LUMINESCENCE DATING OF AEOLIAN DEPOSITS, KEELER, OWENS VALLEY, CALIFORNIA

Jose Luis Antinao, Elizabeth Huenupi, Sophie Baker, Arthur Lewis, Glenn Berger.
Desert Research Institute, 2215 Raggio Parkway, Reno, NV 89512-1095, USA,
[jantinao@dri.edu].

30 Aug 2012
NOTE: Here we report on quartz OSL single-grain dating of sediment of the Keeler area. Four preliminary ages were calculated and reported by Dr. Glenn Berger from samples analyzed between July and September 2011; reported preliminary results are confirmed, and a few notes on interpretation and alternative scenarios are included. The rest of the samples were prepared and run by Dr. Antinao and listed collaborators in July-August 2012, and the ages calculated are reported below.

INTRODUCTION

Ten samples were collected by Dr. Glenn Berger from shallow pits dug on aeolian landforms in the Keeler area in September 2010 (Figs. 1 and 2), with consultation from Nick Lancaster. The goal was to determine the burial age (time of last exposure to daylight) of the sediments in the different sampled units using luminescence dating of single-grain quartz aliquots. Ten primary samples were taken from hand-dug shallow pits (Table 1). Twenty nine other samples were taken from the surroundings of the primary samples in order to measure the environmental ionizing radiation and associated parameters.

Reported here are ages based on the single-grain aliquots, using common assumptions on the sedimentary environment to which they belong and employing statistical analyses widely used in relevant literature. However, for some samples a single unequivocal interpretation of the data is not evident; these samples will be discussed individually.

SAMPLES

The luminescence samples and their settings are listed in Table 1 in the order of their collection by Dr. Berger. Small samples were collected adjacent to and ~20 cm above and below the luminescence samples (Fig. 1). The small samples were employed for measurement of *in situ* and saturation water concentrations, as well as elemental concentrations. These data are required for dose-rate calculations.

Luminescence samples were extracted from cleaned (8-20 cm of surface was first removed) pit walls by use of light-tight tins (8 or 16-oz sizes). Most of the samples were extracted using horizontal insertion of the tin into a cleaned wall (Fig. 2). A few of them were collected by cleaning a 15-20 cm wide bench or pedestal where the tin was then inserted vertically. In all cases, only the ends of the sediment sample within each tin were exposed to light during sampling. Consequently, ~1.5 cm of this end material was removed under filtered

(dim orange) laboratory lighting before processing of the interior sample for luminescence measurements.

LUMINESCENCE-DATING METHODS

Optically-stimulated-luminescence (OSL) dating (also 'optical' or 'photonic' dating) determines the time since the last exposure to daylight of quartz and/or feldspar grains in unheated sediments (Berger, 1986; Aitken, 1998; Rhodes, 2011), and therefore provides a unique dating tool for Quaternary sediments. OSL is very sensitive to daylight, with removal of as much as 90% of the quartz signal possible in only 5-15 s of full sunlight exposure. However, single grains are not always exposed to full sunlight when transported in fluvial or sheet-wash systems, or if transport occurs in darkness. Thus, in water-borne sediment, one can typically expect a mixed-age population of grains even without post-depositional mixing of sediment. The advent of single-grain dating procedures, where the aliquot size is reduced to a single grain of quartz or feldspar, eliminates the need to assume that all grains experienced lengthy daylight exposures before burial. By using statistical analysis of a population of grains, as long as the mechanisms of deposition are well established from the sedimentology and pedological features of the deposit, the grains that were not completely bleached at deposition can be isolated from the population and therefore those grains supplying a true burial dose of the last sedimentary (burial) event can be identified. In the case of this report, the event of interest is related to the last aeolian sedimentation in the area.

Quartz was chosen in favor of feldspar for these dating experiments because feldspar grains can often contain an unstable component of luminescence (anomalous fading) that can lead to age underestimates (e.g., Aitken, 1998). Sand size grains were used rather than silt sized grains because silt is more likely to move vertically within the profile which gives rise to mixed age grain populations within a given stratum as reported by Berger et al. (2004). Furthermore, in the case of sand size fractions, it is possible to isolate quartz because the coarser grains can withstand chemical and physical treatments that allow separation of the different minerals.

The basic principles of luminescence dating are outlined here. After burial, low-level, ambient ionizing radiation (mainly from the decay of K, U and Th isotopes within the sediment) provides an effectively constant (over the few thousands of years of interest for this study) dose rate (D_R) to buried mineral crystals. This ionizing radiation dislodges electrons from lattice-mineral sites into lattice charge traps (either light-sensitive or not), some of which can be stable over more than a million years. Under optical stimulation in the laboratory a fraction of the trapped light-sensitive charges recombine with opposite charges at certain lattice sites, releasing photons. The intensity of this OSL is proportional to the time since last daylight exposure, which in suitable settings is equivalent to the last burial time. This naturally occurring OSL is measured in the laboratory, along with the sensitivity of the sample (OSL signal response to an applied radiation dose). These data yield a paleodose (D_E or 'equivalent dose' measured in units Gy or Gray) which is a measure of the total absorbed energy from ionizing radiation that is stored in the crystal since the last daylight exposure. The dose rate – the annual rate of storage of ionizing-radiation energy in the crystal (D_R, measured in Gy/ka) – is also measured in the laboratory and/or in the field. Thus, the burial age of the sample may be calculated as $t = D_E/D_R$ in calendar years.

The dose rate for these samples was determined by analysis of the sediment surrounding the sample using ICP-MS to determine the K content and thick-source-alpha-particle counting

(e.g., Huntley et al., 1986) to determine the U and Th contributions to the dose rate. The burial dose rate will not be constant if there have been radioisotope decay-series disequilibria in the deposits (e.g., Olley et al., 1996), but this is uncommon. Furthermore, alpha counting is more accurate in the presence of disequilibrium than are the more commonly used procedures that determine only the concentrations of the parent nuclides (e.g., neutron activation methods or ICP-MS for U and Th, as well as K content).

Measurement of the D_E or paleodose is performed using the single-aliquot-regenerative-dose (SAR) OSL procedure (Murray and Wintle, 2000, 2003), which is now an established method for dating quartz-bearing silts and sands (reviews by Bøtter-Jensen et al. 2003; Feathers, 2003; Duller, 2004; Roberts et al., 2005; Lian and Roberts, 2006; Jacobs and Roberts, 2007; Rhodes, 2011). A typical SAR protocol may comprise about seven steps for each aliquot, in which the natural OSL signal is measured and then scaled/calibrated by exposing the sample to regenerative doses of increasing magnitude and measuring the resulting OSL signals so that a growth curve of signal to dose can be constructed (Fig. 3). Each SAR cycle also incorporates a sensitivity assessment by including a small uniform test dose and second OSL measurement immediately after the regenerative dose is administered and its OSL signal measured.

Most quartz grains release two to four OSL signal components, each having different release rates (e.g., Jain et al., 2003, 2005). The preferred component for SAR dating is the 'fast' component (e.g., Wintle and Murray, 2006), a signal usually released in the first 0.8 s of typical blue-diode stimulation or the first 0.1s of the laser stimulation used in these single-grain experiments (Fig. 4). A dating precision of ca. 10% (sometimes better) can be attained routinely with multi-grain SAR quartz methods (e.g., Murray and Olley, 2002) applied to eolian sand. The SAR age range for quartz generally is from as little as 8 years (e.g., Ballarini et al., 2003, 2007) to ca. 150 ka (Murray and Olley, 2002) for normal-radioactivity sediment.

All samples in this study have been dated by the single-grain approach to the SAR-OSL procedure (e.g., Duller, 2004, 2008; Berger et al., 2009), in the case where each aliquot consists of only a single grain (or very few). Sand grains are inserted into a 10x10 grid of precision holes within anodized aluminum discs that are placed in the platter positions in the luminescence reader. The DRI laboratory employs discs having either 300 µm diameter x 300 µm deep holes (for grains 150-225 µm in diameter) or 200x200 µm holes (for grains <150 µm in diameter). Within the automated micro-focused green-laser instrumentation, up to 48 discs of 100 holes each (thus 4800 holes) can be analyzed in one experiment. Although it has many advantages, single grain dating also has some challenges that need to be mentioned. One of the main issues is that the proportion of 'bright' quartz grains to dim ones is variable, ranging from as little as <1% to more than 20% depending on the geological setting. Depending on the observed D_E distribution, the history of the sediment being dated, and to what extent intrusion of younger grains by bioturbation was minimized by choice of sampling points, a population of about 20-100 single grain D_E values are required for good statistics in the evaluation of the sample D_E. In this study, viable D_E values from as few as 20-30 grains out of 1200 measured grains was considered acceptable. The results shown below demonstrate that in the Keeler area samples, the quartz-bearing fraction has a favorable yield of only 2-3%.

A 'transformed-probability-density' (TPD) plot (Berger, 2010) is employed here to visualize the D_E data obtained from SAR dating experiments. This plot is analogous to a histogram plot, but having a kind of 'weighting', wherein the least precise or largest-error-bar D_E values have the least probability of representing age-estimate components. Technically the form of the plot proposed by Berger (2010) is not a probability plot but rather is a type of weighted

frequency plot. This plot can be used when D_E values are > 0 and when the absolute errors in D_E values appear to increase with D_E value (i.e., the relative errors are roughly similar or constant). Thus the weighting is by inverse variance of the relative errors, not by inverse variance of the absolute errors. A TPD plot is superior to a conventional histogram plot because a histogram plot is appropriate only when all data have equal errors, which is rare with SAR dating. This concept is illustrated in Figure 5, which shows data plotted in a familiar (unweighted) histogram plot. Here the eolian sample (inset) has essentially one age component. That is, there is a tight, effectively Gaussian (statistically 'normal') distribution of D_E values. On the other hand, for the fluvial sample, many grains will retain a relict-age signal (they are not exposed to much or any daylight during final transport to the burial horizon), leading to a positively skewed distribution. In this case, only the D_E values defining the lowest-D_E (lowest age) cluster (component) yield the true burial age. D_E distributions are presented as TPD plots below (e.g., Figs. 6-8,10-11), as a visual aid to recognizing the presence and range of any cluster of 'youngest-age' D_E values and thus as a visual aid for deciding which method to use for the calculation of a D_E value in the estimation of a sample burial age.

LUMINESCENCE-DATING PROCEDURES

Quartz-rich fractions were prepared as follows: Any carbonates and organic material were destroyed by use of 1N HCl acid and 30% H_2O_2, respectively, (with de-ionized water rinses between and after). Frantz (S.G. Frantz, Inc., www.sgfrantz.com) isodynamic magnetic separation was employed to obtain non-magnetic subfractions which were then treated with 48% HF acid for dissolution of feldspars (e.g., Aitken, 1998).

After HF acid treatment, representative multigrain portions of each sample were tested for the possible presence of residual feldspar ('contamination') by first administering a 10 Gy radiation dose, and then, after a 2 day delay, stimulating with infrared radiation (IR) at 80°C (only feldspar responds to such IR stimulation). If a sample was significantly contaminated and if enough sample remained, the HF treatment was repeated. In this project, samples OWN10-5, -9 and -10 required a second HF treatment. Based on the sample size after these first steps of preparation, certain samples were chosen for full OSL analysis. Samples OWN10-1, -7 and -8 were considered too small to be processed further at this stage.

For the single-grain SAR experiments, 62-90, 90-150 or 185-225 µm size fractions of purified quartz were used depending on availability in the sampled sediment. Discs with a hundred 300 µm holes were loaded under dim filtered red-orange light. Luminescence measurements were made using TL-DA-20 Risoe automated readers at the Division of Earth and Ecosystems Sciences within DRI, in Reno. All quartz OSL measurements were made in the UV range using a Hoya U340 filter at 125 °C. The grains were stimulated with the focused beam of a 10 mW Nd:YVO_4 solid state diode-pumped laser emitting 532 nm wavelength (green) radiation, following 10s preheats for both natural and regenerative doses as described in Table 3. Key features of the SAR runs include (a) use of a 40s-50°C IR 'wash' step (e.g., Olley et al., 2004) at the start of each SAR cycle to ensure that any remaining small feldspar signal was removed or minimized from the run data (even though the post-HF IR multi-grain tests showed negligible feldspar contamination); (b) use of the 40-s 'blue-diode wash' step of Murray and Wintle (2003) to ensure total bleaching at the end of each cycle; (c) use of a zero dose SAR cycle after the largest regenerative dose cycle to test for thermal transfer and recuperation; (d) use of a recycling

ratio test, comprising a final SAR cycle whereby a regenerative dose identical to the first one administered is given, allowing a further test of the sensitivity correction procedure.

In order to determine the range of test doses required to create a growth curve for each sample before the full SAR testing was performed on the single-grain discs, a brief D_E test was carried out on each sample. This involved measuring the approximate magnitude of the natural dose on three multi-grain test aliquots per sample. Test aliquots were prepared by mounting grains on aluminum discs using silicon oil spray (~100 grains per disc, using a 2 mm mask on 9.8 mm discs).

In addition to the experiments aimed to determine suitable test doses for the SAR cycles, we ran sensitivity tests to choose the total number of discs needed to yield a reasonably large spread of D_E values, guided by the concepts outlined by Olley et al. (1999), but small enough to avoid unnecessarily long run times. Between 9 and 45 discs were used, with an absolute minimum of 9 discs (i.e. 900 grains).

The quality-control criteria employed to accept or reject OSL signals and the resultant SAR D_E values from grains were similar to those in common practice (e.g., Wintle and Murray, 2006). The most important criterion was that the D_E value fell well inside the regenerative doses used. In a few cases, additional SAR cycles with higher regenerative doses were performed on the grains so this criterion was fulfilled.

After observation of the shape of the D_E distribution histograms, the distributions were analyzed using either the Central Age Model (CAM) or a Minimum Age Model (MAM) (3- or 4-parameter) (Galbraith et al., 1999) or their corresponding un-logged versions (Arnold et al., 2009), which were used when values were close to zero or negative. For analyzing profile likelihoods, to determine if additional components were present in the distribution, data analysis procedures using scripts in R (Arnold et al., 2009) and Matlab (Cunningham and Wallinga, 2012) were used (e.g. Fig.9).

RESULTS

Dose-rate data are listed in Table 2 with details in footnotes. Dose rates are typically 2-4 Gy/ka for most terrestrial sediments (Aitken, 1985, 1998), and in the case of these samples they range from 3.53 to 4.23 Gy/ka. Calculated D_E values and ages are listed in Table 3, also with details in footnotes. The OSL age estimates range from ca. 35 to 1700 years (before 2011). The interpretative basis for these different age estimates is discussed below, with explanations for the choice of model D_E used to obtain each age estimate.

DISCUSSION

OWN10-2

A well resolved youngest-age population is evident in the D_E distribution (solid black circles in Figure 6). Although CAM age estimates could be obtained for this sample, it was preferred to apply a MAM to the distribution given the significant proportion of partially bleached grains shown by the ‘tail’ of the distribution. The preferred age for this sample using an un-logged 4-parameter MAM is 35±4 years (before 2011) (Table 3).

OWN10-3

The preferred un-logged 3-parameter MAM age estimate for this sample (81±25 years

before 2011) is based on 23 D_E values. A few higher D_E values (Table 3; Fig. 7) may represent grains that were poorly bleached during deposition.

OWN10-4

The preferred 3-parameter MAM age estimate for this sample (1710±250 years before 2011) is based on 30 D_E values (Table 3). A broad tail in the observed distribution (not shown here) represents grains that were poorly bleached during deposition, similar to OWN10-3.

OWN10-5

TPD plots for OWN10-5 provide a 3-parameter MAM age estimate for this sample of 727±130 years (Table 3), estimated using a D_E value of 2.88±130 Gy based on 61 grains. This sample displays a broad tail distribution similar to OWN10-4.

OWN10-6

TPD plots for this sample (Fig. 8) do not clearly show a youngest-age population of grains. Overlapping young populations can be discriminated with the relative profile likelihood plot (Fig. 9). We favored use of the youngest set of D_E values (~0.15 Gy) rather than the next likelihood maxima at ~0.24 Gy to estimate the un-logged 3-parameter MAM age for this sample, yielding 40±20 ka. Use of the other possible value would increase the age by ~24 years.

OWN10-9

TPD plots for OWN10-9 (Fig. 10) were used to determine an un-logged 3-parameter MAM age estimate for this sample of 172±72 years (Table 3), based on 31 grains. In a similar way to the other young samples in the study, this sample displays a well-defined distribution indicating that a minimum age model best represents the value of D_E.

OWN10-10

TPD plots for this sample (Fig. 11) do clearly show a youngest-age population of grains. An older population can be seen at ~4.4 Gy. This observation is captured accurately by the un-logged 4-parameter MAM model age, which gives an age estimate of 423±45 years, and yields also a model for the partially bleached population of normally distributed D_E values at $(\mu,\sigma)=(4.43,0.5)$ Gy.

GENERAL OSL CHARACTERISTICS OF THE DATED SAMPLES

In most of these samples, only 1-2% of the quartz grains are bright and have OSL properties that allow extraction of a growth curve. This is similar to other environments in the eastern Sierra Nevada that have been analyzed by single-grain OSL of quartz (e.g., Ophir Creek, Berger, 2011). All require a large amount of single-grain discs to be loaded and measured before a reasonable age estimate can be made.

All samples display D_E populations that show some degree of partial bleaching. Grain bleaching is less complete in conditions of fast deposition. In the case of these aeolian sediments, it is possible that some of the transport occurred during short high intensity storms rather than in steady winds. Sedimentological and geomorphologic features of these landforms will help clarify the depositional environment of the sediments.

CONCLUSIONS

Seven samples were dated using green laser optically stimulated luminescence of single-grain aliquots of quartz in the 62-225 μm fraction of aeolian sediments collected in the Keeler area. Obtained ages are in the range expected, bounding these deposits between ca. 35 and ~1700 years before 2011AD.

Acknowledgements

NSF grants to Dr. Glenn Berger supported the acquisition of the OSL readers and associated equipment. The authors thank the Desert Research Institute (DRI) for continuing support of the infrastructure of DRI's E.L. Cord Luminescence Geochronology Laboratory.

REFERENCES

Adamiec, G., & Aitken, M.J. (1998). Dose-rate conversion factors: Update. Ancient TL, 16, 37-50.

Aitken, M.J. (1985). Thermoluminescence Dating: Academic Press, San Diego, 351 p.

Aitken, M.J. (1998). Introduction to Optical Dating: Oxford University Press, Oxford, 256 p.

Arnold, L.J., Roberts, R.F., Galbraith, S.B., and DeLong, S.B. (2009). A revised burial dose estimation procedure for optical dating of young and modern-age sediments: Quaternary Geochronology, 4(4), 306–325.

Ballarini, M., Wallinga, J., Wintle, A.G., & Bos, A.J.J. (2007). A modified SAR protocol for optical dating of individual grains from young quartz samples, Radiation Measurements, 42, 360-369.

Ballarini, M., Wallinga, J., Murray, A.S., van Heteren, S., Oost, A.P., Bos, A.J.J., & van Eijk, C.W.E. (2003). Optical dating of young coastal dunes on a decadal time scale. Quaternary Science Reviews, 22, 1011-1017.

Berger, G.W. (1986). Dating Quaternary deposits by luminescence -- recent advances. Geoscience Canada, 13, 15-21.

Berger, G.W. (1988). Dating Quaternary events by luminescence, *In* Easterbrook, D.J., ed., Dating Quaternary Sediments: Geological Society of America, Special Paper 227, p. 13-50.

Berger, G.W., Henderson, T.K., Banerjee, D., & Nials, F.L. (2004). Photonic dating of prehistoric irrigation canals at Phoenix, Arizona. Geoarchaeology, 19, 1-19.

Berger, G.W. (2010). An alternate form of probability-distribution plots for D_E values. Ancient TL 28(1), 11-21.

Berger, G.W. (2011). Annual Report for Grant NSF-EAR-1015665: Optical single-grain dating of debris flows.

Bøtter-Jensen, L., McKeever, S.W.S., & Wintle, A.G. (2003). Optically Stimulated Luminescence Dosimetry. Elsevier, New York, 350 pp.

Cunningham, A.C. and Wallinga, J. (2012). Realizing the potential of fluvial archives using robust OSL chronologies, Quaternary Geochronology, Available online 9 June 2012, ISSN 1871-1014, 10.1016/j.quageo.2012.05.007.

Duller, G.A.T. (2004). Luminescence dating of Quaternary sediments: recent advances. Journal of Quaternary Science, 19, 183-192.

Feathers, J.K. (2003). Use of luminescence dating in archaeology. Measurement Science and Technology, 14, 1493-1509.

Galbraith, R.F. (2005). Statistics for Fission Track Analysis. Chapman and Hall/CRC, Interdisciplinary Statistics Series, 224 pp.

Huntley, D.J., & Wintle, A.G. (1981). The use of alpha scintillation counting for measuring Th-230 and Pa-231 contents of ocean sediments. Canadian Journal of Earth Sciences, 18, 419-432.

Huntley, D.J., Nissen, M.K., Thompson, J., & Calvert, S.E. (1986). An improved alpha scintillation counting method for determination of Th, U, Ra-226, Th-230 excess and Pa-231 excess in marine sediments. Canadian Journal of Earth Sciences, 23, 959-969.

Jacobs, Z., & Roberts, R.G. (2007). Advances in optically stimulated luminescence (OSL) dating of individual grains of quartz from archaeological deposits. Evolutionary Anthropology, 16, 210-223.

Jain, M., Murray, A.S., & Bøtter-Jensen L. (2003). Characterization of blue-light stimulated luminescence components in different quartz samples: Implications for dose measurement. Radiation Measurements, 37, 441-449.
Jain, M., Murray, A.S., & Bøtter-Jensen, L. (2005). A single-aliquot regenerative-dose method based on IR (1.49 eV) bleaching of the fast OSL component in quartz. Radiation Measurements, 39, 309-318.
Lian, O.B., & Roberts, R.G. (2006). Dating the Quaternary: progress in luminescence dating of sediments. Quaternary Science Reviews, 25, 2449–2468.
Mejdahl, V. (1979). Thermoluminescence dating: beta-dose attenuation in quartz grains. Archaeometry, 21, 61-72.
Murray, A.S., & Olley, J.M. (2002). Precision and accuracy in the optically stimulated luminescence dating of sedimentary quartz: a status review. Geochronometria, 21, 1-16.
Murray, A.S., & Wintle, A.G. (2000). Luminescence dating of quartz using an improved single-aliquot regenerative-dose protocol. Radiation Measurements, 32, 57-73.
Murray, A.S., & Wintle, A.G. (2003). The single-aliquot regenerative dose protocol: potential for improvements in reliability. Radiation Measurements, 37, 377-381.
Olley, J.M., Murray, A.S., & Roberts, R.G. (1996). The effects of disequilibria in the uranium and thorium decay chains on burial dose rates in fluvial sediments. Quaternary Science Reviews (Quaternary Geochronology), 15, 751-760.
Olley, J.M., Caitcheon, G.G., & Murray, A. (1998). The distribution of apparent dose as determined by optically stimulated luminescence in small aliquots of fluvial quartz: Implications for dating young sediments. Quaternary Science Reviews, 17, 1033-1040.
Olley, J.M., Caitcheon, G.G., & Roberts, R.G. (1999). The origin of dose distributions in fluvial sediments, and the prospect of dating single grains from fluvial deposits using optically stimulated luminescence. Rad. Measurements, 30, 201-217.
Olley, J.M., Pietsch, T., & Roberts, R.G. (2004). Optical dating of Holocene sediments from a variety of geomorphic settings using single grains of quartz. Geomorphology, 60, 337-358.
Prescott, J.R., & Hutton, J.T. (1994). Cosmic ray contributions to dose rates for luminescence and ESR dating: large depths and long-term time variations. Radiation Measurements, 23, 497-500.
Rhodes, E.J. (2011). Optically Stimulated Luminescence Dating of Sediments over the Past 200,000 Years. Annual Reviews in Earth and Planetary Sciences, 39, 461-488.
Roberts, R.G., Morwood, M.J., & Westaway, K.E. (2005). Illuminating Southeast Asian prehistory: New archaeological and paleontological frontiers for luminescence dating. Asian Perspectives, 44, 293-319.
Wintle, A.G., & Murray, A.S. (2006). A review of quartz optically stimulated luminescence characteristics and their relevance in single-aliquot regeneration dating protocols. Radiation Measurements, 41, 369-391.

TABLE 1. Luminescence Samples

Sample ID	Depth [cm]	Location	Context	Expected Age [a]
OWN10-1	100	Roadcut	Sand deposit, uniform	Late Holocene-Historic
OWN10-2	100	Hand-dug pit below mud-crack surface	Sand deposit, covering silty clay horizon with cobbles in it	Late Holocene-Historic
OWN10-3	125	Hand-dug pit below mud-crack surface	Sand deposit, uniform	Late Holocene-Historic
OWN10-4	73	Hand-dug pit below mud-crack surface	Sand deposit, uniform up to ~1m depth then coarser sand deposit	Late Holocene-Historic
OWN10-5	50	Hand-dug pit below mud-crack surface	Sand deposit, uniform	Late Holocene-Historic
OWN10-6	90	Hand-dug pit below mud-crack surface	Sand deposit, uniform	Late Holocene-Historic
OWN10-7	55	Hand-dug pit below mud-crack surface	Sand deposit, uniform	Late Holocene-Historic
OWN10-8	45	Hand-dug pit below mud-crack surface	Sand deposit, uniform	Late Holocene-Historic
OWN10-9	43	Hand-dug pit below mud-crack surface	Sand deposit, uniform	Late Holocene-Historic
OWN10-10	67	Hand-dug pit below mud-crack surface	Sand deposit, uniform	Late Holocene-Historic

[a] Glenn Berger (field notes, 2011).

TABLE 2. Dose rates for the samples.

Sample [a]	Water [b]	K_2O [c] (%)	C_t [d] ($ks^{-1} \cdot cm^{-2}$)	C_{th} [d] ($ks^{-1} \cdot cm^{-2}$)	D_{CR} [e] (Gy/ka)	Dose rate [f] (Gy/ka)
OWN10-2	0.12±0.02	3.11±0.05	0.656±0.009	0.303±0.028	0.22±0.02	3.53±0.14
	0.20±0.08	3.06±0.05	0.632±0.012	0.251±0.020		
OWN10-3	0.05±0.02	3.33±0.05	0.721±0.010	0.324±0.030	0.22±0.02	4.23±0.19
	0.05±0.08	3.20±0.04	0.592±0.006	0.243±0.016		
OWN10-4	0.05±0.02	3.07±0.05	0.638±0.008	0.243±0.024	0.21±0.01	3.84±0.10
		3.20±0.10	0.587±0.028	0.276±0.020		
OWN10-5	0.05±0.02	3.23±0.05	0.630±0.006	0.284±0.018	0.22±0.01	3.96±0.10
		3.10±0.05	0.667±0.014	0.332±0.022		
OWN10-6	0.07±0.02	3.20±0.05	0.612±0.008	0.285±0.025	0.20±0.01	3.81±0.10
		3.01±0.05	0.647±0.006	0.265±0.020		
OWN10-9	0.006±0.002	3.27±0.05	0.464±0.005	0.168±0.015	0.24±0.02	3.82±0.05
	0.005±0.008	3.15±0.04	0.505±0.004	0.233±0.014		
OWN10-10	0.029±0.005	3.55±0.05	0.499±0.007	0.267±0.022	0.24±0.02	4.02±0.13
	0.019±0.008	3.63±0.04	0.548±0.005	0.236±0.015		

[a] The first row of data for each sample comprises data for sediment immediately surrounding the primary sample and is used to calculate the β contribution to the dose rate, while the second row represents data for samples taken 10-30 cm away from the primary sample, used to calculate the γ dose-rate component.

[b] Weight of water/weight of dry sample. Values were estimated from data for soils on similar landforms at similar climatic settings and considering the maximum saturated value and (as a minimum) the field moisture content determined for samples in the laboratory.

[c] The potassium value for material around the quartz grains. The internal K is set to zero for dose-rate calculation, and an empirically estimated internal dose rate for typical quartz is added later (footnote *f*). The estimated uncertainty is ±0.05%; when averaging subsamples, errors were added in quadrature.

[d] Total and thorium count rates from finely powdered samples for thick-source-alpha-particle-counting (TSAC) method (Huntley and Wintle, 1981). $C_u = C_t - C_{th}$. These values are inserted directly into the age equations of Berger (1988), with the internal-quartz dose-rate components set to zero (see footnote *f*).

[e] A cosmic ray component estimated from the algorithm of Prescott and Hutton (1994) (basically, a function of burial depth, with depth estimates from Table 1). An estimated uncertainty of ±0.02 was used.

[f] Calculated with the conversion factors given by Adamiec and Aitken (1998), using the equations of Berger (1988). The attenuation of β rays across the sand grain is accounted for using attenuation factors from Aitken (1985). An estimated small internal dose-rate in quartz of 0.05±0.03 Gy/ka (Murray, pers. comm., 2004) is added to the calculated dose rate.

TABLE 3. SAR data and apparent ages for the sand samples.

Sample	Grain size [a] (μm)	Preheat / cut heat [b] (˚C)	Statistical model [c]	D_E [d] (Gy)	Age Estimate [e] (yr before 2011)
OWN10-2	62-125	180/160	ulMAM4 (93/3100)	0.124±0.014	35±4
OWN10-3	185-225	220/200	ulMAM3 (23/900)	0.341±0.105	81±25
OWN10-4	62-90	180/160	MAM3 (30/3100)	6.54±0.95	1710±250
OWN10-5	105-150	180/160	MAM3 (61/4500)	2.88±0.51	727±130
OWN10-6	62-90	180/160	ulMAM3 (41/2500)	$0.153^{+0.077}_{-0.068}$	40±20
OWN10-9	185-225	220/200	ulMAM3 (31/1200)	0.654±0.273	172±72
OWN10-10	185-225	220/200	ulMAM4 (21/1200)	1.70±0.18	423±45

[a] Grain size attenuation factors for the beta-dose were taken from Mejdahl (1979).

[b] For the SAR approach, preheat temperatures (Murray and Wintle, 2000), held for 10 s. A signal-readout temperature of 125˚C was employed.

[c] Statistical modeling used to analyze D_E distributions shown in the TPD plots. Number of useful and total grains is indicated as a ratio, in parentheses. MAM: minimum age model, with 3 or 4 indicating 3-parameter or 4-parameter models; ul: unlogged.

[d] D_E value obtained by modeling the D_E distribution data.

[e] D_E divided by dose rate from Table 2.

FIGURES

Figure 1 (left). OWN10-2 sampling pit. Metal cans are shown inserted into the wall. The OSL sample was taken with the large can and subsamples for dose-rate determinations correspond to the smaller 1 oz cans.

Figure 2 (right). OWN10-3 sampling pit. The OSL sampling can is shown inserted into the pit wall. The general setting for most of the sampled sediment pits is similar to that shown in this photograph, with preserved stratigraphy and sedimentary structures, and minimal pedogenic or biogenic disturbance on the section.

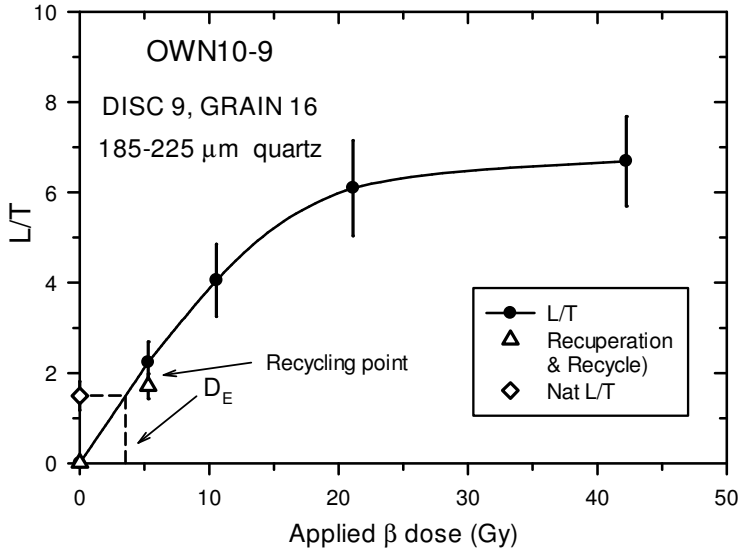

Figure 3. SAR growth curve of L/T ratios for disc 9, grain 16 of sample OWN10-9, showing the interpolation of the y-axis L_n/T_n ratio (sensitivity corrected natural signal) and the resultant D_E value (vertical line, in this example ~3.8 Gy). Interpolated polynomial curve is shown only for illustrative purposes. Note that recuperation should be close to zero, and recycling ratios close to 1 to accept an aliquot for further data processing. Error bars are ±1σ.

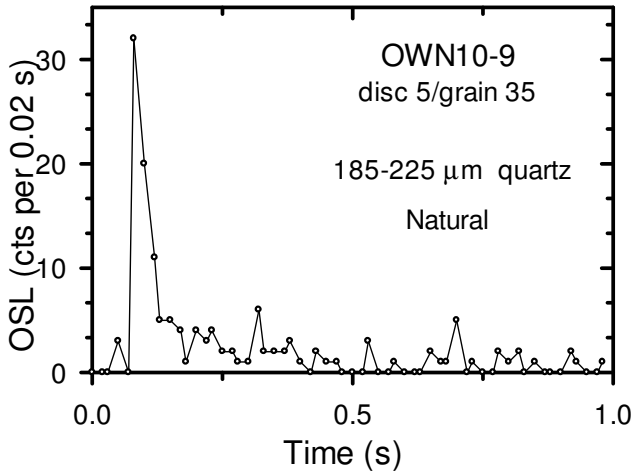

Figure 4. Shine curve for the natural (L_n) signal, before any laboratory radiation dose, from disc 5, grain 35 of sample OWN10-9. Note the characteristic shape of luminescence by quartz. The first 5 data points record a signal before the laser is turned on, while the subsequent 4 points represented the laser stimulated signal (points 6-9). Net OSL signal was calculated by subtracting from this initial signal a background signal using the last 10 data points. For each shine curve the net signal is used in calculation of the normalized (L/T ratio) signal. The corresponding test-dose (T) shine (normalization shine) is not shown.

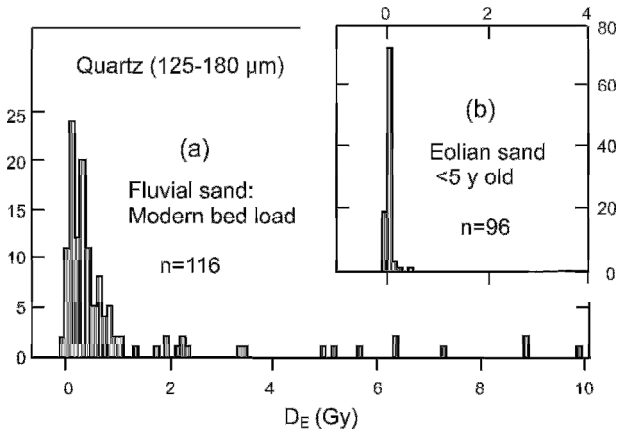

Figure 5. Histograms of D_E values for small (60-100 grains) single aliquots of quartz grains from: (**a**) a modern fluvial bed-load sand, and (**b**) a modern (< 5 y) eolian sand (modified from Olley et al., 1998). Here the eolian sample (inset) has essentially one age component. That is, there is a tight, effectively Gaussian (statistically 'normal') distribution of D_E values. On the other hand, for the fluvial sample, many grains will retain a relict-age signal (they are not exposed to much or any daylight during final transport to the burial horizon), leading to a positively skewed distribution. In this case, only the D_E values defining the lowest-D_E (lowest age) cluster (component) yield the true burial age.

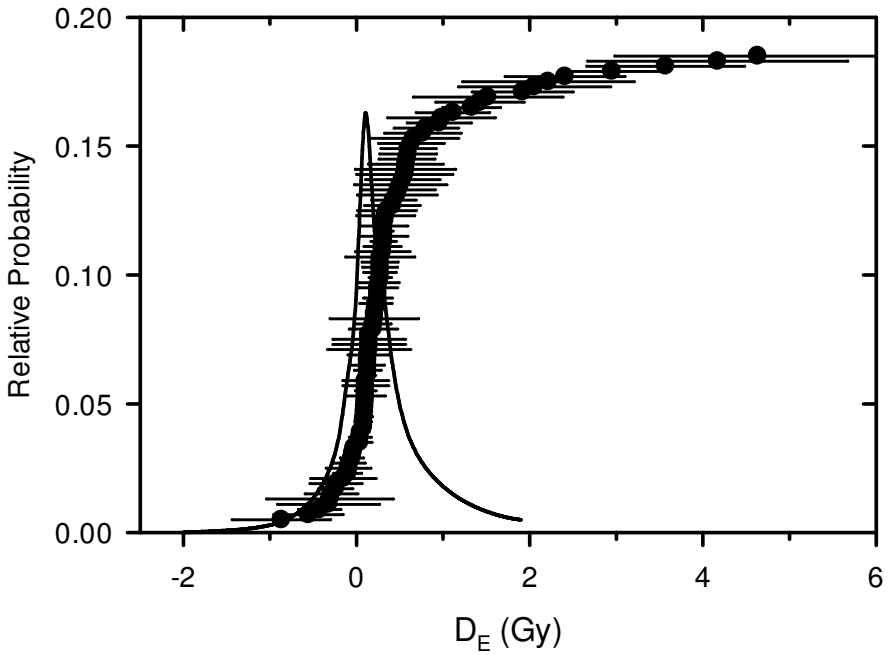

Figure 6. Transformed probability distribution (TPD) curve (solid curve) for sample OWN10-2, showing the ranked series of D_E values and errors obtained from the 93 grains that yielded reliable values. Note that the Keeler area samples are all expected to have young ages, and therefore the signal is very close to the background, resulting in some grains returning negative values for D_E. In these cases, un-logged versions of statistical models are used.

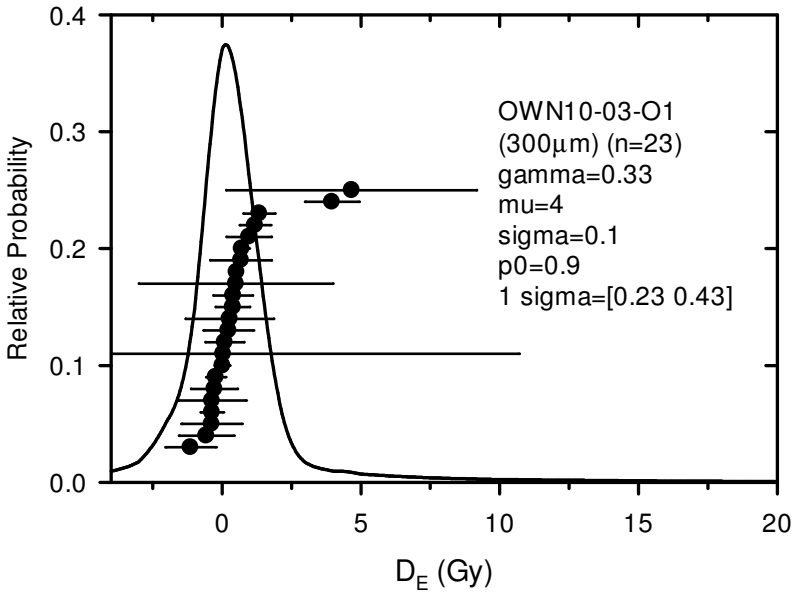

Figure 7. TPD plot and ranked D_E values for sample OWN10-3. O1 denotes the first output of values analyzed with the software Analyst 3.4.2. Values returned by the un-logged 3-parameter minimum age model (Galbraith, 2005; Arnold et al., 2009) are shown in the inset text. Note that the variable *gamma* returned by the R script of this model and shown in the inset text corresponds to the actual D_E estimate.

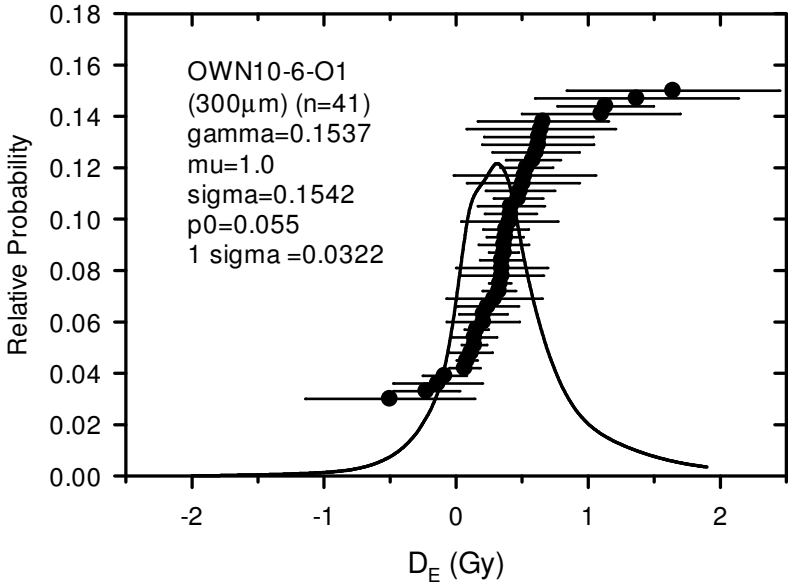

Figure 8. TPD plot and ranked D_E values for sample OWN10-6. Note that the variable *gamma* returned by the R script of this model and shown in the inset text corresponds to the actual D_E estimate.

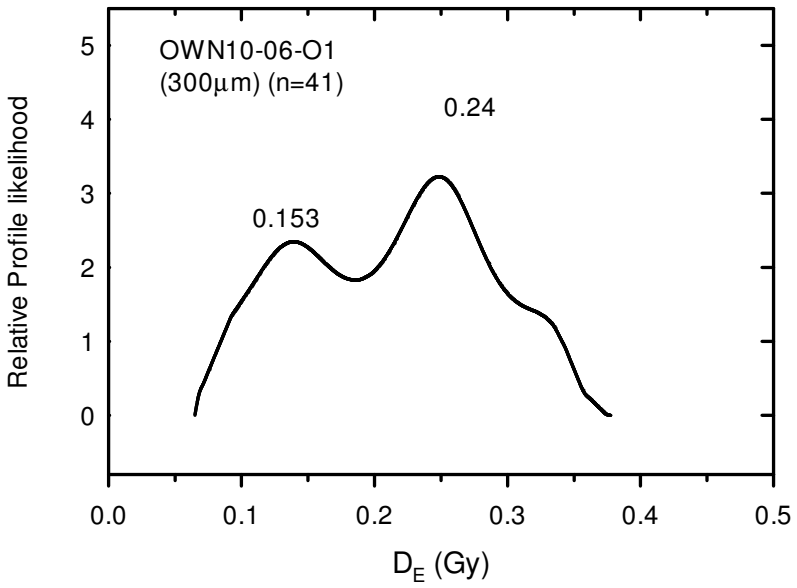

Figure 9. Relative profile likelihood for the D_E distribution as modeled by using a 3-parameter minimum age model (Cunningham and Wallinga, 2012) for sample OWN10-6. Note the two maxima indicating two close possible solutions for a minimum age, from which the lowermost was used.

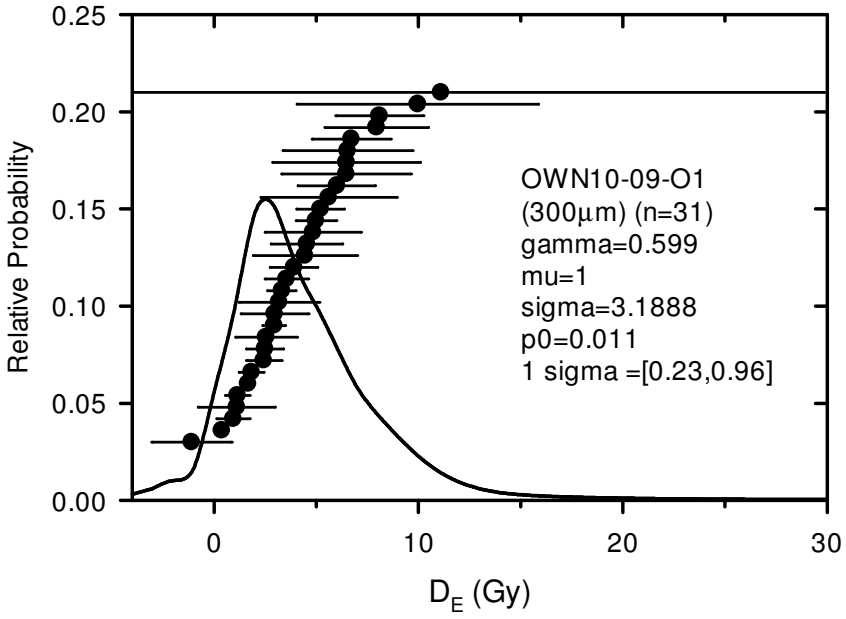

Figure 10. TPD plot and ranked D_E values for sample OWN10-9. Note that the variable *gamma* returned by the R script of this model and shown in the inset text corresponds to the actual D_E estimate.

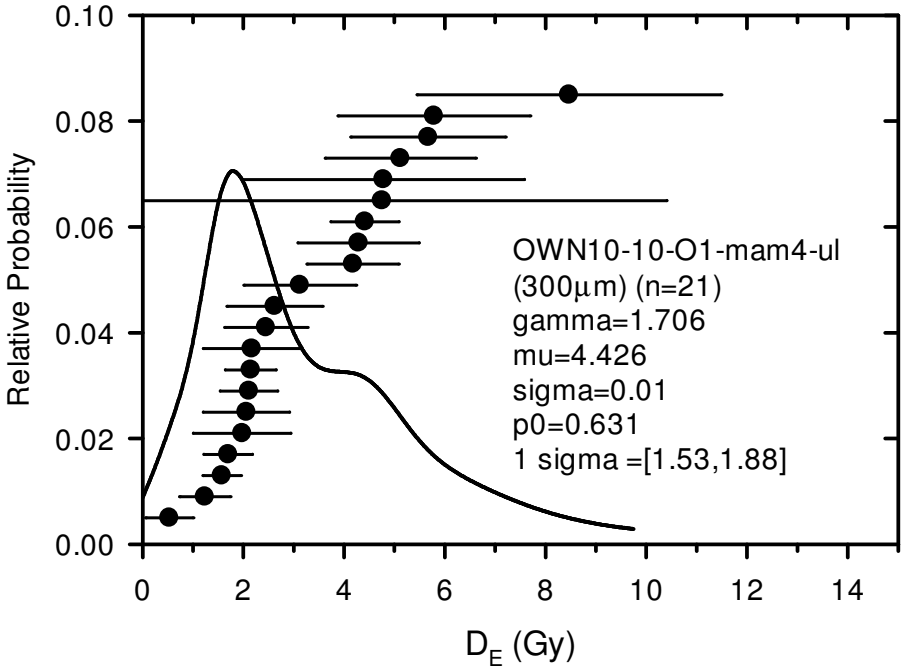

Figure 11. TPD plot and ranked D_E values for sample OWN10-10. The inset text shows the results of a run of the 4-parameter un-logged MAM age model (Arnold et al., 2009). Two previous runs using the 3-parameter un-logged MAM age model using the entire distribution and a series of central age model runs using the ~2 Gy subset of D_E values gave similar results, but the result shown was preferred because it modeled well the distribution of poorly bleached grains (to the right, with a mean around ~4.4 Gy). Note that the variable *gamma* shown in the inset text corresponds to the actual D_E estimate used to calculate the age estimate.